

VISCOUS FLOW MODELING USING THE VORTEX PARTICLES METHOD

HENRYK KUDELA AND ZIEMOWIT MIŁOSZ MALECHA

*Wroclaw University of Technology,
Faculty of Mechanical and Power Engineering,
Wybrzeże Wyspiańskiego 27, 50-370 Wroclaw, Poland
{henryk.kudela, ziemowit.malecha}@pwr.wroc.pl*

(Received 7 October 2008; revised manuscript received 5 December 2008)

Abstract: The vortex particle method is an easy and attractive tool to analyze flow phenomena by investigating vorticity fields and the generation of vorticity at solid walls. The vorticity generation at the walls and its introduction to the flow is of fundamental significance for understanding such phenomena as transition to turbulence, boundary layer separation in an eruptive way, and vortex structures regeneration. In the present study the vortex-in-cell usefulness of the method has been tested using a variety of simple test problems: the Poiseuille flow, the second Stokes problem, the cavity, the backward step flow, the vortex dipole interaction with the wall, and the flow past a square cylinder in the vicinity of a wall in order to illustrate the correctness and usefulness of the vortex particle method.

Keywords: vortex-in-cell method, vorticity generation, eruption

1. Introduction

Vorticity is fundamental for fluid mechanics. All real flows are characterized by vorticity different from zero. A great number of phenomena in hydrodynamics is analyzed from the point of view of vorticity dynamics. The great significance and importance of the discrete vortex methods for the study of hydrodynamic phenomena stems that. Vortex methods have been used to model hydrodynamic phenomena for a long time. Rosenhead (1933, [1]) has been acknowledged as one of the first users. He approximated the surface of discontinuity with point vortices between two incompressible fluids with different tangent velocities and studied its evolutions. Such a surface can be considered as a vortex sheet layer and it is known that it is unstable (Kelvin-Helmholtz instability). Other scientists that followed him tried to use vortex methods to model some different hydrodynamic phenomena [2, 3]. However, it was Chorin's [4] works that finally propelled the studies of vortex methods application to an unbelievable degree. In his work [4] Chorin proposed a discrete vortex method, called the vortex bubble method. The point vortex was replaced by a vortex with a finite support. He designed the method in such a way that viscous flows

could be modeled without a numerical mesh application. He used a viscous-splitting algorithm, whose solution was obtained in two steps: first, the inviscid fluid equation was solved, then the Stokes problem (diffusion equation) was solved by taking into account the fluid viscosity. Calculations were carried out in Lagrange variables. The boundary non-slip condition on rigid walls was found by generating new vortices on the wall. Although Chorin demonstrated the method's efficiency for a model flow past a cylinder, the method required some more arbitrary procedures – for example, it should be controlled, if the circulation value of new vortices generated on the cylinder boundary is not too large by selecting the cut-off radius of a vortex bubble. The method proposed by Chorin belongs to direct methods. The velocities of vortex particles are calculated on the basis of the Biot-Savart law [5, 6] by summarizing velocities induced by all particles in the flow. The number of operations in each discrete time step is proportional to $O(N^2)$ where N denotes the number of particles in the flow.

A special, fast method of summation for calculating the interaction of particles that are presented in the computational domain [7, 8] should be used to reduce the time calculation. A different approach, which allows the time of calculations to be reduced by hundreds of times, is the Euler-Lagrange approach called vortex in cell (VIC) [9]. The approach retains the key feature of particle methods. Advection is dealt with using Lagrangian variables but the velocity is determined by solving the Poisson equation for the stream function by using a numerical grid. In this way, explicit discretization of the advective term in the Navier-Stokes equation and related stability constraints are avoided. The values from the grid nodes are interpolated onto the positions of particles. The grid may be used also for the fluid viscosity simulation.

The question arises: Is it possible for a discrete vortex method to be a certain, fully reliable numerical method to model viscous flows? The terms „fully reliable method” means a method that is simple to use, with a number of minimum parameters which influence the computational accuracy without referring to any additional arbitrary means and whose numerical solution converges to the exact solution when the numerical grid is refined. In [4, 10], the VIC method accuracy was compared with the finite difference and spectral method. In the present work, using many different, relatively simple examples, we have tried to demonstrate that the vortex particle method is accurate and that it is possible to determine its order. It is worth underlining that the method is especially attractive when it comes to analyzing the evolution of vorticity.

2. Equations of fluid motion

Equations of the incompressible and viscous fluid motion have the following form:

$$\frac{\partial \mathbf{u}}{\partial t} + (\mathbf{u} \cdot \nabla) \mathbf{u} = -\frac{1}{\rho} \nabla p + \nu \Delta \mathbf{u}, \quad (1)$$

$$\frac{\partial u}{\partial x} + \frac{\partial v}{\partial y} = 0, \quad (2)$$

where $\mathbf{u} = (u, v)$ is the velocity vector, ρ is the fluid density, ν is the kinematic viscosity, p is the pressure and $\Delta = \partial^2/\partial x^2 + \partial^2/\partial y^2$ is the Laplace operator. Further,

we will assume that $\rho = \text{const}$. Equations (1) and (2) should be completed with boundary and initial conditions which in this case have the following form:

$$\mathbf{u} = u_w \text{ for } (x, y) \in \partial\Omega, \quad (3)$$

$$\mathbf{u}(x, y, t = 0) = \mathbf{u}_0(x, y), \quad (4)$$

where $\partial\Omega$ denotes the rigid wall movement with velocity u_w and $\mathbf{u}_0(x, y)$ is an initial velocity distribution. Equation (2) which expresses fluid incompressibility, guarantees the existence of stream function ψ and is related to the velocity field in the following way: $u = \partial\psi/\partial y$, $v = -\partial\psi/\partial x$. In the two dimensional space, vorticity vector $\text{rot}(\mathbf{u}) = k\omega = \partial v/\partial x - \partial u/\partial y$ has only one nonzero component perpendicular to the plane of motion (k is a unit vector perpendicular to the plane of motion). Acting with the rotation operator $\text{rot}(\cdot)$ on both sides of Equation (1), it can be transformed into a Helmholtz equation describing the vorticity field evolution in time:

$$\frac{\partial\omega}{\partial t} + u\frac{\partial\omega}{\partial x} + v\frac{\partial\omega}{\partial y} = \nu\Delta\omega, \quad (5)$$

$$\Delta\psi = -\omega, \quad u = \frac{\partial\psi}{\partial y}, \quad v = -\frac{\partial\psi}{\partial x}. \quad (6)$$

Vectorial Equation (1) has been replaced by a scalar Equation (5) for $\omega(x, y, t)$. It is worth noticing that there is no pressure term in Equation (5). A viscous splitting algorithm is commonly used in the vortex methods [5]. This means that Equation (5) is solved in two steps. First, the inviscid equation is solved:

$$\frac{\partial\omega}{\partial t} + u\frac{\partial\omega}{\partial x} + v\frac{\partial\omega}{\partial y} = 0, \quad (7)$$

and then the viscous equation (Stokes problem) follows:

$$\frac{\partial\omega}{\partial t} = \nu\Delta\omega. \quad (8)$$

In the present work, Equation (7) has been solved by the vortex particles method. The diffusion Equation (8) has been solved by the Particle-Strength-Exchange method.

3. Vortex particles method description

This method stems from Equation (7), with the vorticity constant on the trajectory: $\omega(\mathbf{x}(t, \boldsymbol{\alpha}), t) = \omega(\boldsymbol{\alpha}, 0)$, where $\mathbf{x}(t, \boldsymbol{\alpha})$ means the fluid particle position which was at $\boldsymbol{\alpha}$ in the initial time $t = 0$. It is known from the third Helmholtz theorem [6] that vorticity is carried by the fluid. The motion of vortex particles can be described by the following set of differential equations:

$$\frac{d\mathbf{x}}{dt} = \mathbf{u}(\mathbf{x}, t) \quad \mathbf{x}(0, \boldsymbol{\alpha}) = \boldsymbol{\alpha}, \quad (9)$$

where $\boldsymbol{\alpha} = (\alpha_1, \alpha_2)$ denotes the Lagrange coordinates of the fluid particles and $\mathbf{x} = (x, y)$. The velocity $\mathbf{u}(\mathbf{x}, t)$ is determined by the vorticity distribution (see Equation (6)). Velocity in grid nodes can be obtained by solving the Poisson equation for the stream function (6) on a numerical mesh by the finite difference method. Velocity from the mesh nodes is interpolated onto the vortex particles location. Such

an approach speeds up calculations significantly and it has been applied in the present work [11].

For calculation purposes it is necessary to replace the infinite set of ordinary differential Equations (9) with a finite one. In order to do this, the space of Lagrange variables α is covered with a regular mesh $(j_1\Delta x, j_2\Delta y)$ ($j_1, j_2 = 1, \dots, N$), $\Delta = \Delta y = h$. Such a mesh is also used to solve the Poisson equation for the stream function. The initial vorticity field is replaced by a discrete distribution of the vortex particles. The adequate circulation is assigned to each particle:

$$\Gamma_p = \int_{A_p} \omega(x, y) dA \approx h^2 \bar{\omega}, \quad (10)$$

where $A_p = h^2$ denotes the mesh cell area with index p , whereas $\bar{\omega}$ is the vorticity mean value for cell A_p . Vorticity is approximated by the total of the Dirac measures:

$$\omega(\mathbf{x}) \approx \sum_{p=1}^N \Gamma_p \delta(\mathbf{x} - \mathbf{x}_p), \quad (11)$$

where N is the number of vortex particles and δ denotes the Dirac function. The circulation of particles changes in time due to diffusion. Equation (7) in the time interval (t_n, t_{n+1}) is obtained by solving the set of differential equations:

$$\frac{d\mathbf{x}_p(t)}{dt} = \mathbf{u}(\mathbf{x}_p^n(t), t), \quad \mathbf{x}_p(t_n) = \mathbf{x}_p^n, \quad t_n \leq t \leq t_{n+1}, \quad p = 1, \dots, N, \quad (12)$$

and new positions \mathbf{x}_p^{n+1} of the vortex particles give an approximate solution of Equation (7) for time $t = t^{n+1}$:

$$\omega^{n+1}(\mathbf{x}) = \sum_{p=1}^N \Gamma_p \delta(\mathbf{x} - \mathbf{x}_p^{n+1}), \quad \mathbf{x}_p^{n+1} = \mathbf{x}_p(t_{n+1}). \quad (13)$$

The particle strength exchange (PSE) method has been used to solve the diffusion Equation (8).

3.1. Particle strength exchange (PSE) method

The main idea of the particle strength exchange (PSE) method is to approximate the differential Laplace operator with an integral operator which has the following form for two dimensions [5, 12]:

$$\Delta\omega(\mathbf{x}) \cong \frac{1}{\varepsilon^2} \int (\omega(\mathbf{y}) - \omega(\mathbf{x})) \eta_\varepsilon(\mathbf{y} - \mathbf{x}) d\mathbf{y}. \quad (14)$$

Function $\eta_\varepsilon = \varepsilon^{-2} \eta(\mathbf{x}/\varepsilon)$, ($\varepsilon > 0$) is an order r symmetric cut-off of the function which satisfies the following moments conditions:

$$\begin{aligned} \int_{\mathbb{R}^2} x_i x_j \eta(\mathbf{x}) d\mathbf{x} &= 2\delta_{ij} \quad \text{for } i, j = 1, 2, 3, \\ \int_{\mathbb{R}^2} x_i^{k_1} x_j^{k_2} \eta(\mathbf{x}) d\mathbf{x} &= 0 \quad \text{for } k_1 + k_2 = 1 \text{ or } 3 \leq k_1 + k_2 \leq r + 1, \\ \int_{\mathbb{R}^2} |\mathbf{x}|^{r+2} |\eta(\mathbf{x})| d\mathbf{x} &< \infty, \end{aligned} \quad (15)$$

where δ_{ij} – the Dirac symbol ($\delta_{ii} = 1$). Parameter ε should be chosen to satisfy the relation $\varepsilon/h \geq 1$; that is, the supports of the neighboring particles should overlap each other (h – mesh cell size). This overlapping means that each particle should be able to communicate with a specified number of the neighboring particles. Using expression (14), Equation (8) can be replaced by:

$$\frac{d\Gamma_p}{dt} = \nu \varepsilon^{-2} \sum_q (\Gamma_q - \Gamma_p) \eta \left(\frac{\mathbf{x}_p - \mathbf{x}_q}{\varepsilon} \right). \quad (16)$$

The following function with compact support $\eta(\mathbf{x})$ has been chosen in this work:

$$\eta(\mathbf{x}) = \begin{cases} \frac{C}{1+|\mathbf{x}|^2} & \text{for } |\mathbf{x}| \leq 2, \\ 0 & \text{for } |\mathbf{x}| > 2, \end{cases} \quad (17)$$

where $C = 0.835$ has been calculated to satisfy the first condition from Equation (15): $\int |\mathbf{x}|^2 \eta(\mathbf{x}) d\mathbf{x} = 2$ [12]. Function $\eta(\mathbf{x})$ can have infinite support. In such a case, the interaction of each vortex particle with all other particles in the flow domain must be calculated. It means that the time calculation is proportional to $O(N^2)$, where N denotes the number of vortex particles in the flow – which significantly slows the calculation process.

In the case of a function with finite support, computer time calculation is proportional to $O(mN)$, where m means the number of particles encompassed by the cut-off function. Since $m \ll N$ and m is constant, the time calculation is proportional to $O(N)$. The kernel of function (17) encompasses exactly nine neighboring vortex particles ($m = 9$) in the algorithm developed for this work.

3.2. Remeshing

The vortex particle method is a self-adaptive method. Vortex particles tend to gather in flow regions where high velocity gradients occur. On the one hand, it is an advantage. On the other hand, it can cause inaccuracies. Particles can create phantom vortex structures which could significantly alternate the velocity field. It also affects fluid viscosity modeling. To keep calculations precise, vortex particles are ordered by distributing them into a regular mesh (remeshing). Vorticity field information transfer from vortex particles into mesh nodes (redistribution) as well as ordering vortex particles distribution in the flow (remeshing) (6) have been performed using interpolation [5]:

$$\omega_j = \sum_{p=1}^N \Gamma_p \varphi \left(\frac{\mathbf{x}_j - \mathbf{x}_p}{\varepsilon} \right) h^{-2}, \quad (18)$$

where ω_j denotes vorticity in the mesh nodes with j index and p index numbers vortex particles. The following interpolation kernel has been chosen in this work [5, 13]:

$$\varphi(x) = \begin{cases} 1 - x^2, & 0 \leq x < 1/2, \\ (1 - x)(2 - x)/2, & 1/2 \leq x < 3/2, \\ 0, & x \geq 3/2. \end{cases} \quad (19)$$

The interpolation kernel (19) can be used only in an unbounded domain. To avoid problems with vorticity „running out” beyond the calculation domain, it is necessary to use one-sided interpolation kernels as follows (see Figure 1):

$$\varphi(x) = \begin{cases} 1 - \frac{3}{2}x + \frac{1}{2}x^2, & \text{for nodes 1, 2, 3} \\ x(2-x), & \text{for nodes 4, 5, 6} \\ x(x-1), & \text{for nodes 7, 8, 9} \\ 0, & \text{for all other nodes.} \end{cases} \quad (20)$$

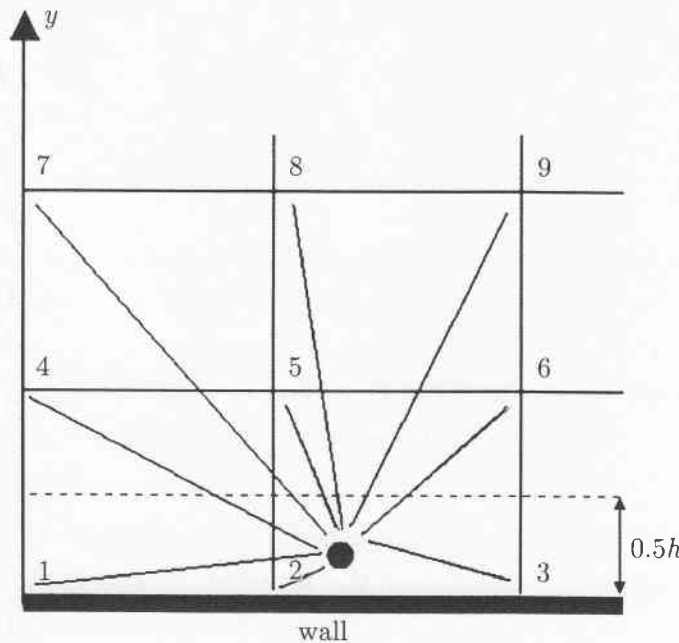


Figure 1. Remeshing for vortex particles close to the wall

Interpolation kernels (19) and (20) maintain a conservation of zero, first and second order moment of the vorticity field:

$$M_a = \int \omega(x)x^a dx = \text{const}, \quad \text{for } a = 0, 1, 2. \quad (21)$$

Both kernels (19) and (20) encompass the nine closest mesh nodes [13].

We decided to do the remeshing for every time step. Therefore, an individual procedure for redistribution of circulation of particles onto mesh nodes was unnecessary. It made the calculations easier and faster. The differential Equations (12) were solved by the second order Euler-improved method. The velocity of the particles between the grid nodes that was needed in the solution of Equation (12) was calculated using the interpolation formula:

$$\mathbf{u}(\mathbf{x}_p) = \sum_j \mathbf{u}_j l_h(\mathbf{x}_p - \mathbf{x}_j), \quad (22)$$

where l_h is a basic bilinear Lagrange's function.

3.3. Implementation of a no-slip condition on a solid wall

The way in which vorticity is generated on the wall has been a scientific problem for a very long time. It is a fact that the wall is the only place in incompressible flows where new vorticity appears [6, 14]. However, a more detailed picture of the process is still not clear. In the practice of vortex methods, we refer to some physical

models or calculation tricks that enable us to determine the vorticity value or vorticity flux on a wall. The first method, the oldest one in historical terms (1933, Thom), which determines the vorticity value on a wall (Dirichlet condition) is often used in calculation methods based on formulating the fluid motion in terms of vorticity and stream function ($\omega - \psi$) [15]. It can be called a calculation method. The other method is based on the dynamic model of vorticity flux generation on the wall (Neumann condition) provided by Lighthill [16]. Both methods have been tested in our work and are presented below.

3.3.1. Dirichlet boundary condition

Condition (3) for a viscous flow equation presents the lack of a fluid slip on the wall. Both the normal component to the wall and the tangent component of the velocity field should equal zero. The description of fluid motion in terms of vorticity and velocity definitely simplified the motion equations, but at the same time it caused problems related to satisfying the no slip condition (3).

For the viscous fluid we found it necessary for the tangent velocity component on the wall to equal the velocity of the wall:

$$u_s = \frac{\partial \psi}{\partial n}, \quad u_s = u_w, \quad (23)$$

where u_s denotes the tangent fluid velocity on the wall, u_w denotes the velocity of the wall, and n denotes the direction perpendicular to the wall. The condition of no penetration of the fluid through the wall (normal speed to the wall equals zero) satisfies the boundary condition for the stream function: $\psi = \text{const}$.

Further, if we apply the five-point differential scheme to the Poisson equation for the stream function (6) it will result in the following equation for points located on the wall:

$$-\omega_{i,0} = \frac{\psi_{i+1,0} - 2\psi_{i,0} + \psi_{i-1,0}}{\Delta s^2} + \frac{\psi_{i,1} - 2\psi_{i,0} + \psi_{i,-1}}{\Delta n^2}, \quad (24)$$

where s denotes the direction tangent to the wall. If Equation (23) is replaced with some finite difference formula for the first derivative and introduced to Equation (24), the value of the vorticity needed to satisfy the non-slip conditions for the fluid on the wall can be obtained. In the present work, we use the most popular – and simplest – Thom formula [15, 17]:

$$\frac{\psi_{i,1} - \psi_{i,-1}}{2\Delta n} = u_w \Rightarrow \psi_{i,-1} = \psi_{i,1} - 2\Delta n \cdot u_w. \quad (25)$$

And since the stream function is constant on the wall $\psi_{i-1,0} = \psi_{i,0} = \psi_{i+1,0}$ the final equation will be:

$$-\omega_{i,0} = -\omega_{\text{wall}} = \frac{2(\psi_{i,1} - \psi_{i,0} - \Delta n \cdot u_w)}{\Delta n^2}. \quad (26)$$

Formula (26) is first order-accurate for vorticity [17]. A table of different higher order formulas can be found in the work [15]. However, as stated in [15] it is hard to point out a formula with the best qualities, nevertheless, we are convinced – and we have already checked it [18] – that a higher order formula should be used for a large Reynolds number value and a more complicated geometry (see also [19]).

In these calculations, raising the order of formula (26) has a very small effect on the numerical results. This is the reason why we have used the Thom formula (26)

to determine the vorticity value on the wall to satisfy the no slip condition (3). If the vorticity is different from that described in Equation (26) – as a result of redistribution of the vortex particles circulation that is present in the flow at the boundary points – then in this node, vorticity is added to preserve Equation (26):

$$\omega_{\text{wall}} = \omega_{\text{old}} + \omega_{\text{add}}, \quad (27)$$

where ω_{old} denotes the vorticity present in the flow, and ω_{add} the vorticity that needs to be added.

Additional vorticity value ω_{add} was determined in the nodes on the walls. This additional vorticity was changed into circulation $\Gamma_{\text{add}} = h^2 \omega_{\text{add}}$ and added to the particles which lay on the wall $\Gamma_{\text{wall}} = \Gamma_{\text{old}} + \Gamma_{\text{add}}$. The number of particles that take part in computations is constant.

3.3.2. Neumann boundary condition

In the other method used in this work the appropriate vorticity flux is determined from the wall into the flow. It corresponds to the boundary condition of the Neumann type and is based on the dynamic description of vorticity provided by Lighthill [16]. The vorticity flux on the wall can be expressed as [20]:

$$\nu \frac{\partial \omega}{\partial n} = -\frac{\gamma(s)}{\Delta t}, \quad (28)$$

where $\gamma = u_s$ is the intensity of the vortex layer along the rigid wall, u_s is the spurious tangential velocity on the wall.

In order to introduce the vorticity caused by an additional vorticity flux into a flow domain, the following initial boundary value problem for a diffusion equation in each time step is solved:

$$\begin{aligned} \frac{\omega_{\text{wall}}}{dt} - \nu \Delta \omega_{\text{wall}} &= 0, \\ \omega_{\text{wall}}(x, y, 0) &= 0, \\ \frac{\partial \omega_{\text{wall}}}{\partial n} &= -\frac{\gamma}{\Delta t \cdot \nu}. \end{aligned} \quad (29)$$

Let us notice that the initial vorticity value equals zero. The vorticity obtained in the mesh nodes by solving problem (29) is changed into circulation and added to the circulation of particles already present in the flow.

In order to get some idea of how a vorticity flux can compensate the spurious tangent component of the velocity field, let us write the viscous flow Equation (1) on the wall:

$$\frac{du}{dt} = -\frac{\partial p}{\partial s} - \nu \frac{\partial \omega}{\partial n} \quad (30)$$

where variable s denotes a derivative in the direction tangential to the wall and n in the normal direction. It can be seen that the acceleration is related to the pressure gradient, as well as to the vorticity flux. Generally the pressure gradient is not known.

If a tangent component of the velocity field different from zero appears on the wall, it can be said that the wall has accelerated in a short time interval Δt :

$$\mathbf{s} \cdot \frac{d\mathbf{u}}{dt} \simeq \frac{u_s(t + \Delta t) - u_s(t)}{\Delta t} = \frac{\gamma(s)}{\Delta t}. \quad (31)$$

We assume that the additional acceleration will be compensated by the additional vorticity flux: $\nu \partial \omega / \partial n$. Hence, it can be assumed that the tangent velocity component in the time interval Δt is balanced as follows:

$$u_s(t + \Delta t) = \nu \Delta t (\partial \omega / \partial n), \quad (u_s(t) \equiv 0). \quad (32)$$

In such a way the vorticity flux can be expressed by formula (28).

3.3.3. Summarizing the computational algorithm of the VIC method

One time step from t_n to $t_n + \Delta t$ proceeds as follows:

- redistribute the particles circulation onto mesh nodes (19), (20);
- solve the Poisson equation for stream function (6);
- calculate the velocity on the numerical mesh;
- fulfill the no-slip condition on solid walls;
- displace the vortex particles according to (12);
- remesh the vortex particles onto a regular grid (formula (19), (20));
- change the circulation of the particles as a result of the diffusion using the PSE method (16).

A fast elliptic solver was used to solve the Poisson equation. The capacitance matrix technique was used to solve the Poisson equation in an irregular region (different from rectangular) [21, 22].

4. Numerical results

4.1. Poiseuille flow

The first test checking if the vortex particle method was correct was the Poiseuille flow in a rectangular duct, for which the velocity distribution is given as follows:

$$\frac{u}{u_{\max}} = 4 \frac{y}{H} \left(1 - \frac{y}{H} \right), \quad (33)$$

where H denotes the height of the duct and u_{\max} is the maximum velocity (in the center line of the duct). The length of the channel is $L = 40$, and the height, $H = 1$.

Figure 2 presents an exemplary solution for $Re = 100$ ($Re = UH/\nu$). In the figure, the vorticity and velocity fields are presented. It can be clearly seen how the initially rectangular velocity profile is changing into a parabolic one due to the presence of the wall as well as to the production and diffusion of vorticity from the wall.

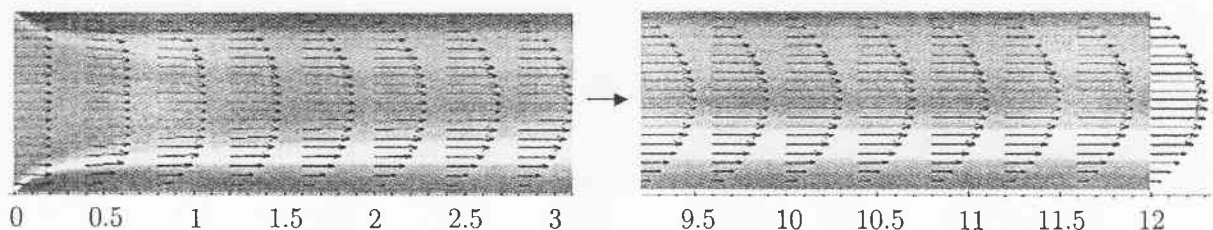


Figure 2. Poiseuille flow – velocity field and vorticity field for $Re = 100$

It is clear from Equation (33) that the solution does not depend on viscosity. The distance on which the velocity profile is formed has been studied in order to investigate the influence of viscosity on the flow entrance effect. It is known from experiments that the length increases with an increase in the Reynolds number [23]. This relationship is approximately linear for the laminar flow: $L_f = C \cdot \text{Re} \cdot H$, where L_f denotes the velocity profile forming length, and C is a constant. Figure 3 presents the results obtained by the authors of this work. In the picture it is seen that the velocity profile formation length depending on the Reynolds number is approximately linear and the constant is $C = 0.075$.

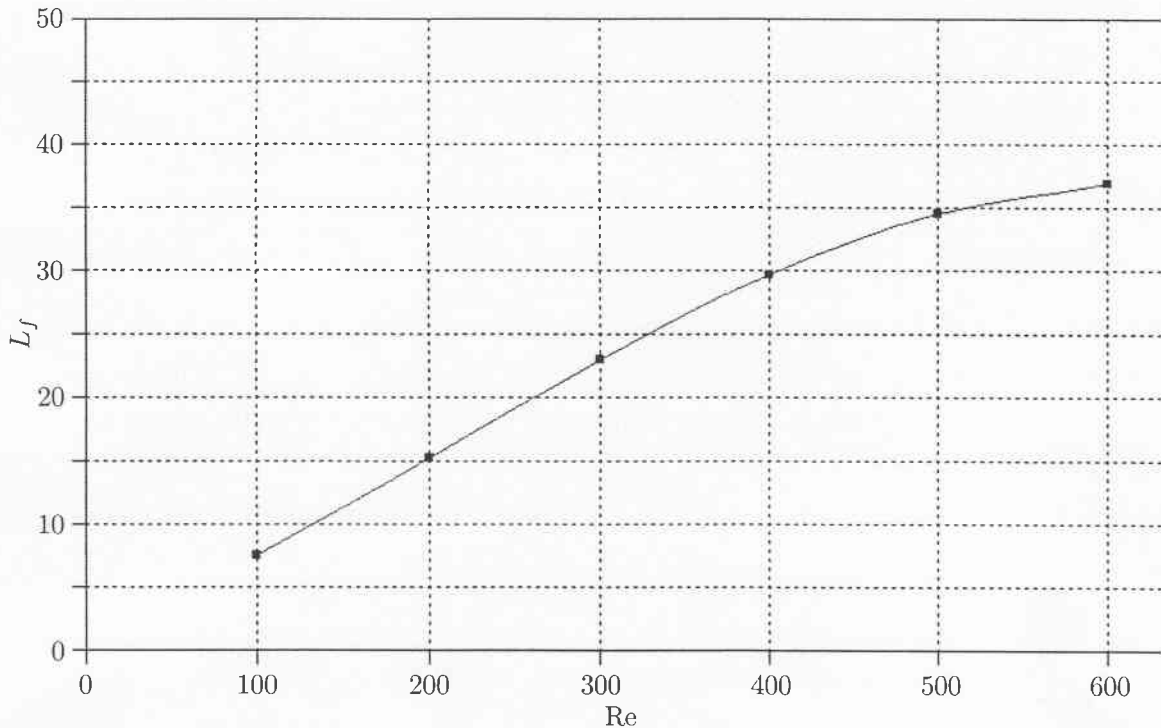


Figure 3. The length of velocity profile formation as dependant on the Reynolds number

Moreover, the order of convergence for the calculation algorithm has been estimated on the basis of the results obtained. To examine the order of convergence the maximum norm has been used for the channel end:

$$\|E(u, u^h)\|_{\infty} = \max_{y,t} |u(y, t) - u^h(y, t)| \leq Ch^{\alpha}, \quad (34)$$

where α , denotes the method order, and h is the numerical mesh size. The calculations have been performed on numerical meshes with a different mesh size $\Delta x = \Delta y = h$ and time step $\Delta t = 0.5h$ in order to obtain the order of convergence. In Figure 4 the convergence of the method is presented graphically. In Figure 4 the dependence on the mesh size on the logarithmic scale is presented. The slope (direction coefficient) of the line reflects the convergence method order. The order of convergence for generation of vorticity is approximately $\alpha \cong 2.0$, and $\alpha \cong 1.5$ when obtained by the method with the Dirichlet boundary condition (Method I) and with the Neumann condition (Method II), respectively.

4.2. Second Stokes problem

A more demanding problem for which an analytical solution is also known is the second Stokes problem [23]. The basic difficulty is a moving wall which oscillates

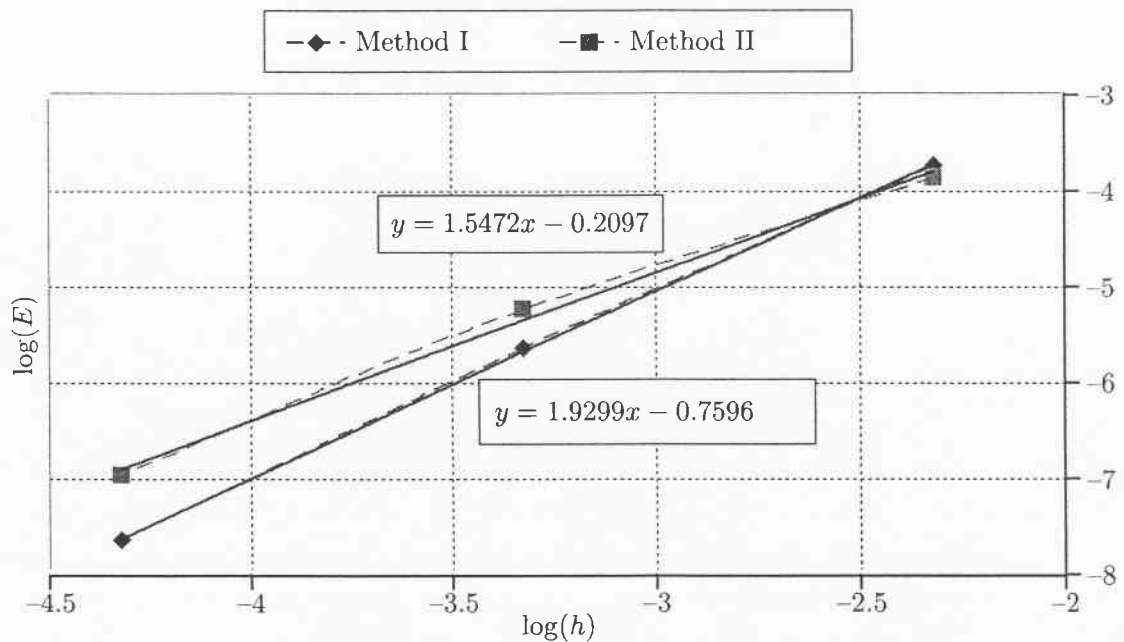


Figure 4. Convergence of the presented method

with a given frequency. The velocity on the wall (boundary condition) is given by the formula: $u(y=0, t) = U_0 \cos(\omega t)$, where U_0 is the velocity of the wall (amplitude) and ω in this case denotes the frequency (it has been assumed that $\omega = 1$). The analytical solution to the second Stokes problem is given by the following equation:

$$u(y, t) = \cos(t - y\sqrt{1/2\nu}) \exp(-y\sqrt{1/2\nu}). \tag{35}$$

Figure 5 presents an example of a solution to the problem discussed for $Re = 400$, $\omega = 1$ and $U_0 = 1$. The computational domain has been taken as: length, $L = 4$, and height $H = 5$. The grid parameter and time step has been used as in the Poiseuille problem. Velocity and vorticity fields can be seen in Figure 5a, whereas frame 5b presents a comparison of the velocity profile obtained by means of the present calculations with the particular solution for time $t = 13$.

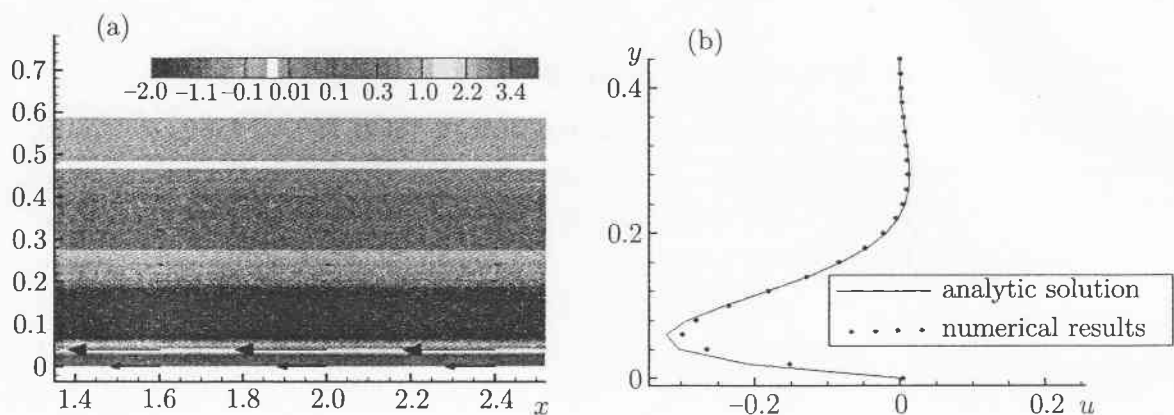


Figure 5. Second Stokes problem: (a) vorticity field and velocity vectors; (b) comparing the horizontal velocity component of the present results with an analytic solution

The order of convergence has been estimated by means of the maximum norm (34) for the middle of the computational domain, $x = 2$. For the generation of vorticity the results are as follows: $\alpha \cong 1.4$ for the boundary condition of the Dirichlet type, and $\alpha \cong 1.3$ for the Neumann condition.

4.3. Cavity flow

The cavity flow has been chosen as the next test problem. The flow in a square cavity with a side length $L = 1$ is caused by the upper wall motion with velocity $u_0 = 1$, while other walls are still. A series of characteristic vortex structures appear in the cavity depending on the Reynolds number $Re = u_0 L / \nu$.

Although there is no analytic solution to this problem, it has been widely used by others to study very different numerical methods [24, 25]. Most often, the position of the primary vortex centre as well as the position of secondary vortex structures are compared in relation to the Reynolds number. We have made a comparison for a wide range of Reynolds numbers and for different sizes of the numerical mesh and with different time step values. The numerical results presented in this work refer to the flow with $Re = 100, 400, 1000, 3200, 5000, 7500, 10000$. The major comparative parameter for the cavity flow is the centre position of the primary vortex (Table 1), and the appearance of secondary vortices. All these phenomena are closely related to the Re number value. Figure 6 shows the flow with the Neumann type boundary condition for vorticity; for the Dirichlet type condition the images are very similar.

The distribution of the obtained streamlines, and the appearance of the characteristic secondary vortex structures as dependent on the Re number are very close to those that can be found in scientific literature.

Table 1. Comparison of the center location in the primary vortex

Re	Present method I (x, y)	Present method II (x, y)	Ghia <i>et al.</i> [24] (x, y)
100	(0.6163, 0.7360)	(0.6164, 0.7336)	(0.6172, 0.7344)
1000	(0.5310, 0.5650)	(0.5310, 0.5638)	(0.5313, 0.5625)
3200	(0.5185, 0.5386)	(0.5185, 0.5386)	(0.5165, 0.5469)
5000	(0.5178, 0.5340)	(0.5165, 0.5337)	(0.5117, 0.5352)
10000	(0.5160, 0.5298)	(0.5159, 0.5273)	(0.5117, 0.5333)

4.4. Flow over backward-facing step

The flow over backward-facing step has been carefully examined both numerically [8, 26–28] and experimentally [29], and owing to that it can serve as a good comparative test. The results obtained in the present research have been compared with the results of the experiments presented by Armely *et al.* [29], as well as with other numerical results obtained by other calculation methods.

A characteristic feature of the over backward-facing step flow is the recirculation zone generated behind the step, which increases with the increasing Reynolds number. The normalized length of this recirculation zone $L = x/H_s$, as dependent on the Re number serves as a comparative parameter (H_s – height of the step). Figure 7 presents the results obtained. An example of the flow field is visible in the image on the left (streamlines and velocity vectors with the vorticity field as a background). A chart from image 7b shows a change of length of the recirculation zone behind the step as dependent on the Reynolds number and a comparison of the present results with experimental and numerical results.

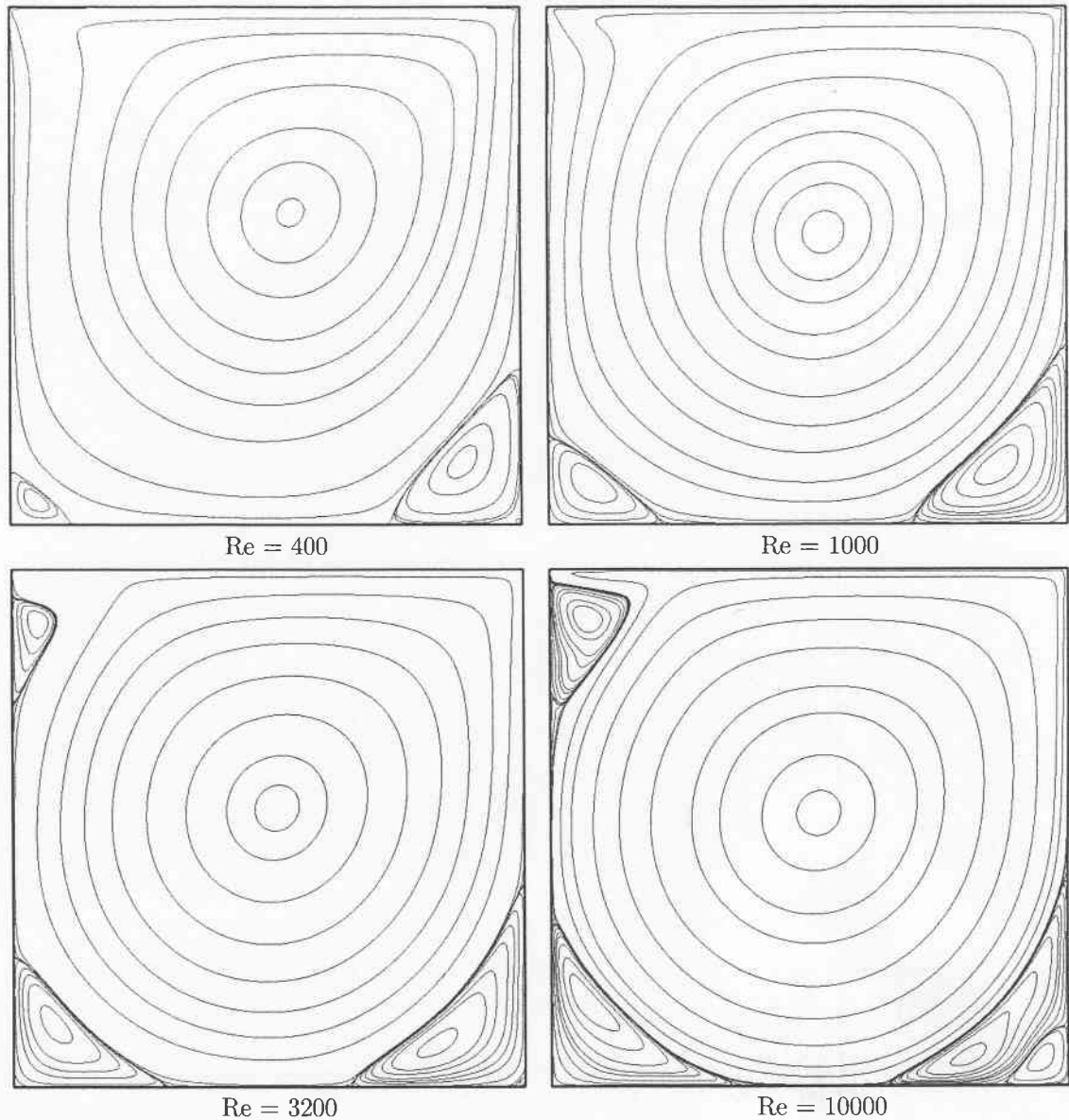


Figure 6. Streamlines for the cavity flow as dependent on the Re number

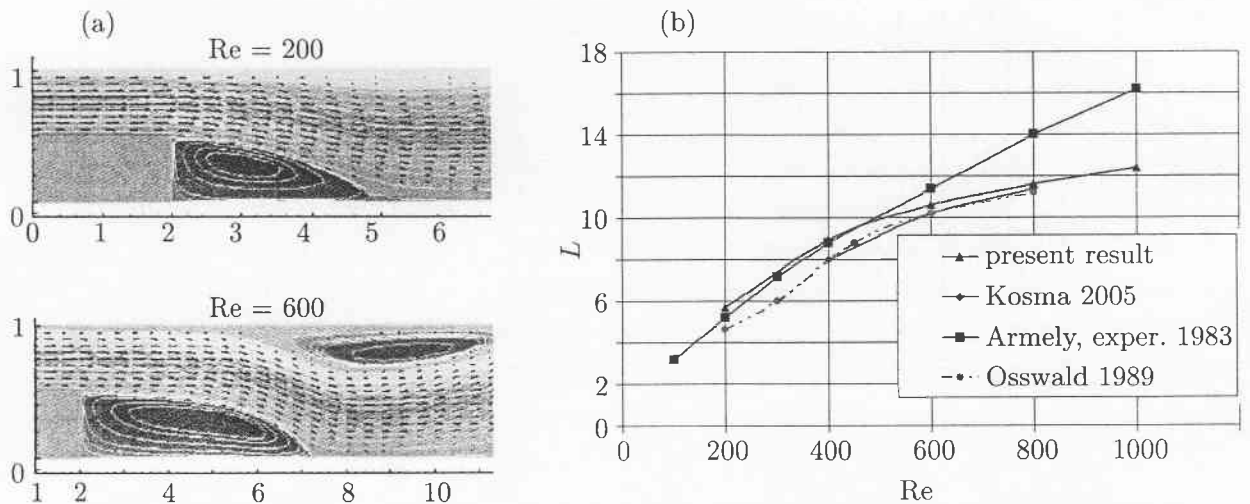


Figure 7. (a) Flow over backward-facing step; (b) the recirculation zone length dependence on the Reynolds number – a comparison of results

A significant concordance for $Re < 600$ of the results obtained in the present work with the experiment can be seen in Chart 7b. For $Re > 600$ it has been noticed in [29] that the flow loses its two-dimensionality and it is the reason for

the discrepancy between the numerical results and the experiment measurements. For a higher Reynolds number, the recirculation zone begins to tear off and a vortex structure similar to the vortex Kármán street (Figure 8) appears in the channel [27].

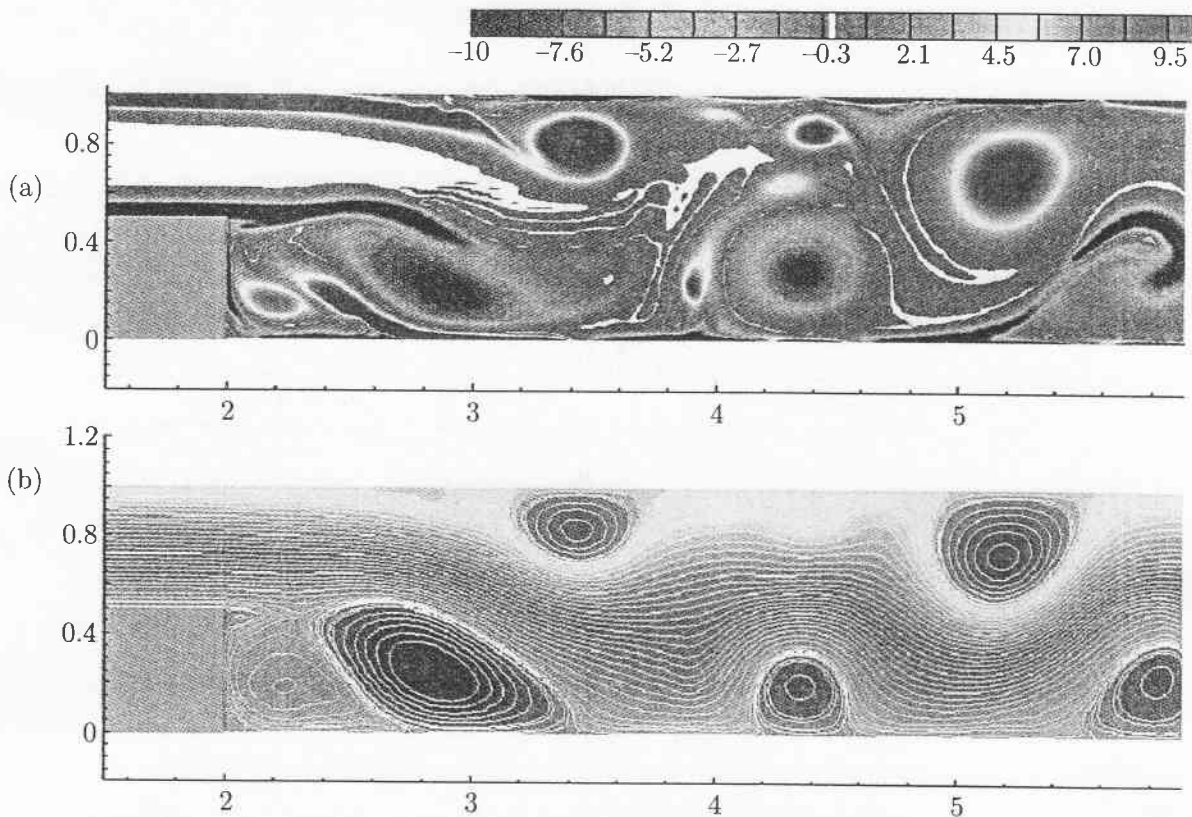


Figure 8. Flow over backward-facing step, $Re = 3000$, $t = 10$: (a) vorticity, (b) isolines of the stream function

4.5. Vortex dipole interaction with a wall

The vortex particle method provides a possibility of examining the motions and interactions of any vortex structures with one another and also with the walls [19, 30]. A vortex dipole interaction with the wall is presented as an example. A vortex dipole is a set of two vortex patches with the same circulation values but with opposite signs which are separated by a small distance from each other.

Figure 9 shows the scheme of a calculation domain with a vortex dipole. At the beginning of the calculations, the fluid was at rest. The calculation area was $L = 5$ long and $H = 5$ high. The boundary conditions for solving the Poisson equation for the stream function were as follows: it was assumed that the velocity and vorticity fields were periodical in direction x whereas for the lower ($y = 0$) and upper ($y = 5$) boundary it was assumed that $\psi = 0$. The no slip condition between the fluid and the wall was determined using the Dirichlet condition for vorticity.

The initial dipole location was defined by two parameters: a – the distance between the centers of patches forming the dipole, b – the distance of the dipole from the wall. The initial radius of the vortex patches was $r = 0.15$, and their initial vorticity values were equal but had opposite signs; the left patch vorticity ω_L was negative (counterclockwise), and the right patch vorticity ω_P was positive (clockwise). Thanks to that, the mutual interaction of dipole patches caused the movement towards the

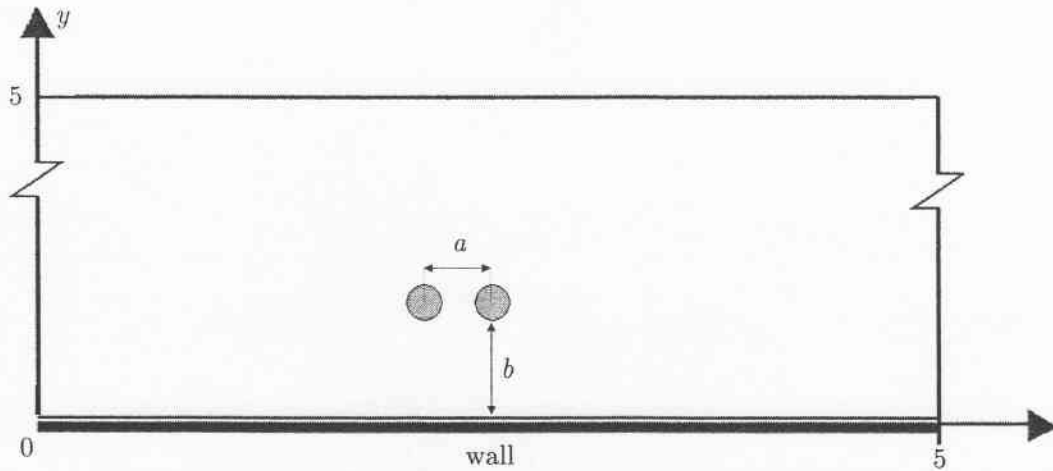


Figure 9. Calculation area of the presented problem

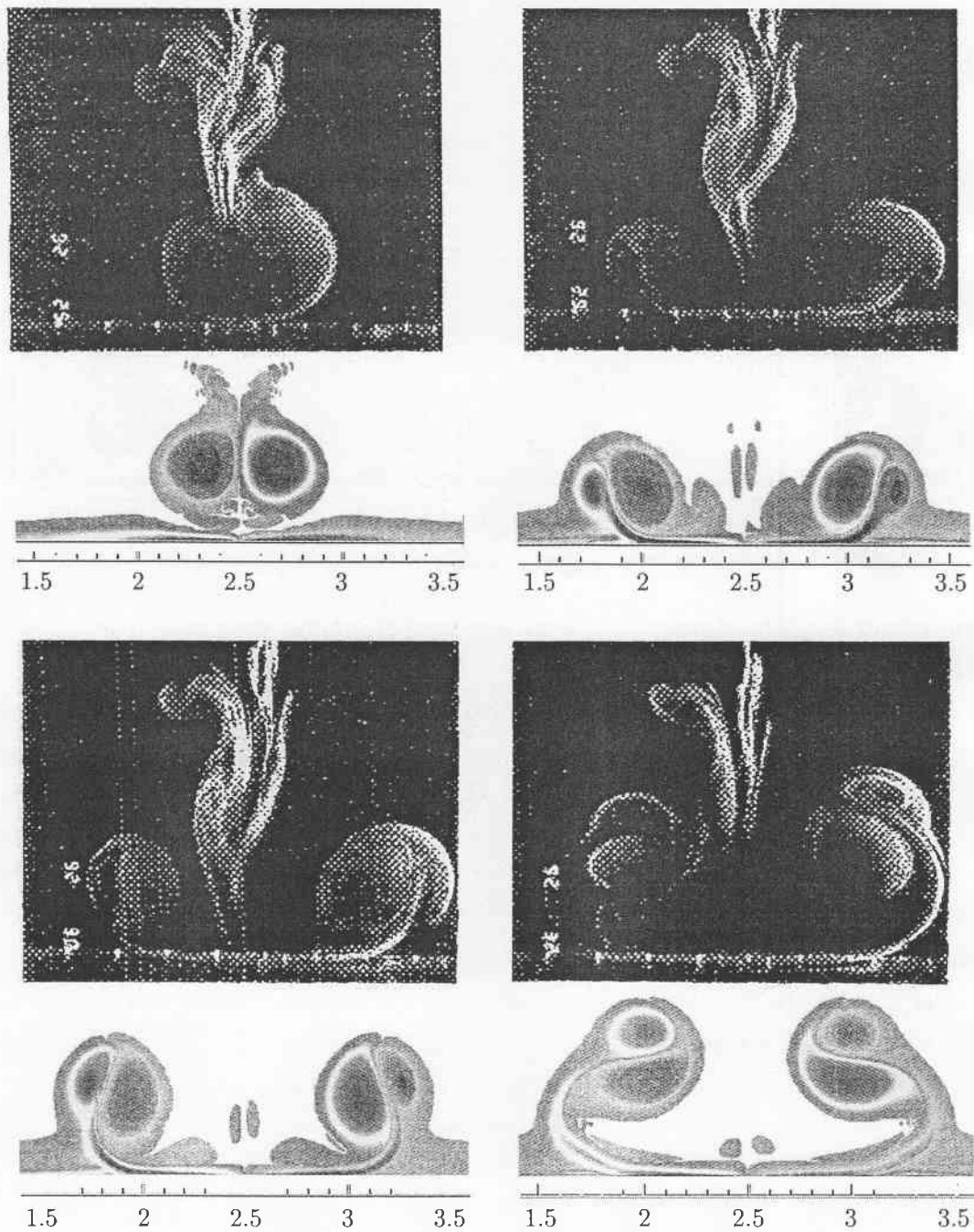


Figure 10. Visualization of a dipole collision with the wall [30] – comparison with numerical results, $\nu = 0.0001$

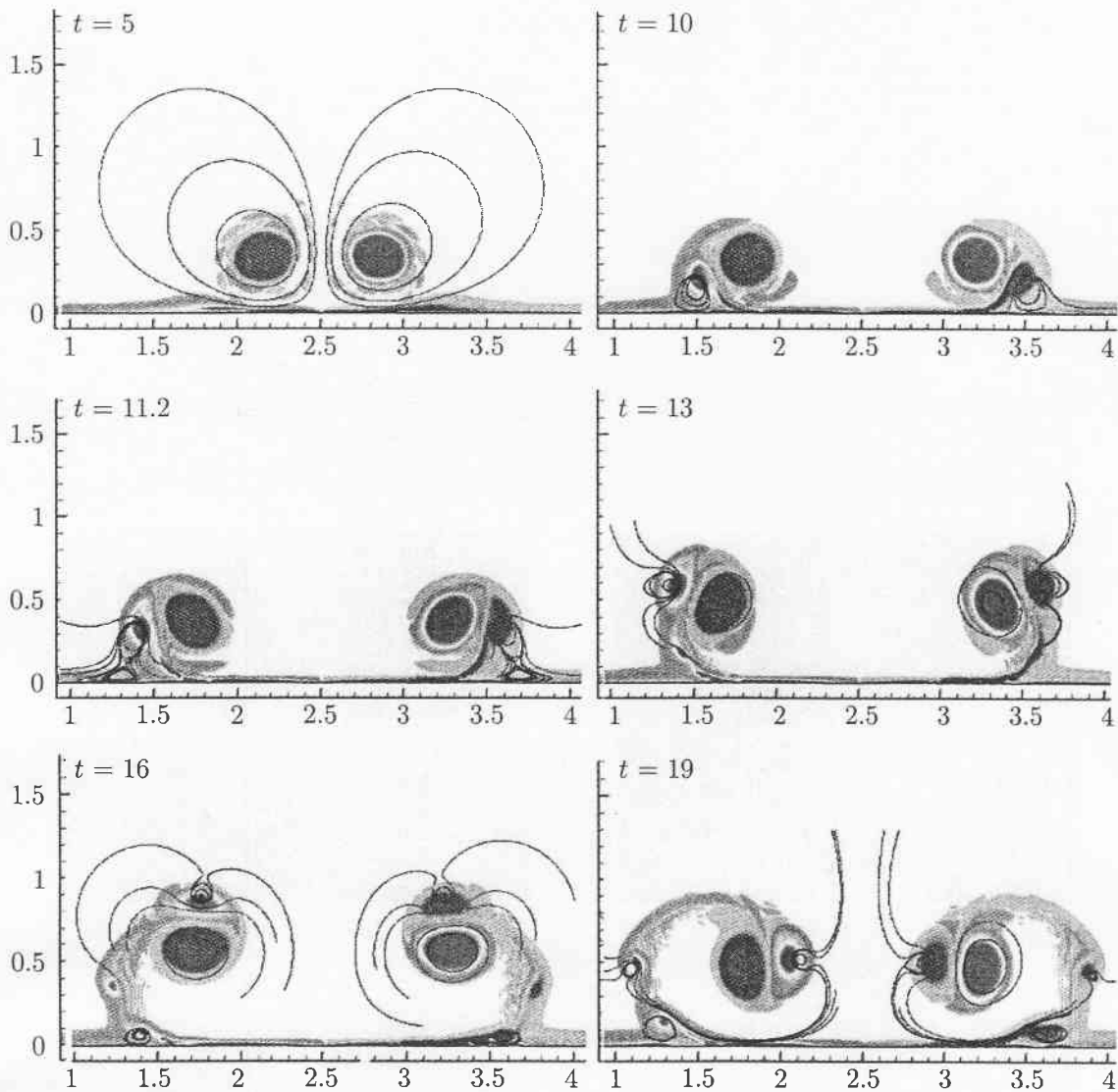


Figure 11. Interaction of the vortex dipole with the wall $\nu = 0.00002$, $a = 0.5$

wall (downwards). The numerical mesh size and the time step were $\Delta x = \Delta y = 0.01$ and $\Delta t = 0.01$, respectively.

The numerical results obtained indicate high agreement with the experiment (Figure 10). Both sizes and locations of the primary and secondary vortex structures are very much alike. Primary structures mean vortex dipole patches, whereas secondary structures are vortices separated from the wall, generated by the interaction of the vortex dipole with the wall. A characteristic feature of vortex dipole interaction with the wall is its rebound from the wall and the appearance of secondary vortex structures.

The picture of the flow for smaller fluid viscosity becomes more complicated. Figure 11 shows the vorticity field with selected streamlines for $\nu = 0.00002$, $a = 0.5$, $b = 0.75$. For time $t = 4$ the primary vortex approaching the wall induces a vortex layer which has the vorticity with the opposite sign with respect to the primary vortices. Then, two recirculation zones (pocket vortices) appear in the wall layer, one on each side ($t = 8$). Then, the pocket vortices are pulled firmly upwards and are torn off ($t = 11.2$). Eruption of the boundary layer takes place [31–34]. Fluid particles from the wall area enclosed in the vortex structure are ejected abruptly

into the flow. The ejected vorticity causes a significant change in the movement of vortex patches. Primary and secondary structures form pairs which are initially lifted upwards together. As the circulation of primary patches is superior to that of the secondary ones, the dipole moves along a curve that approaches the wall again ($t = 13$ to 19). The primary dipole is strong enough to cause separation of other vortices from the wall at its second passage $t = 19$. Then, the vortex patches of the primary dipole move along the wall, increasing the distance from one another. The flow maintains symmetry as a result of a weak mutual interaction of vortex dipole patches.

5. Conclusion

Vortex methods provide natural, useful tools for analyzing the flow in terms of vorticity dynamics. It is one of the few methods which give reasonable results at a wide range of the Reynolds number. The replacing of the non-slip condition for the fluid on the solid boundary flow on the vorticity generation is accurate enough. A very quick and robust alternative method to the grid-based methods is provided using the fast Poisson solvers. The presented methods for 2D can be generalized for three-dimensions [11, 35–37] and numerical results are encouraged. However, the number of papers devoted to three-dimensional applications of the vortex method is by far smaller than for two dimensions. Further work on the three dimensional vortex method application is still needed to obtain some degree of maturity.

Acknowledgements

Both authors wish to acknowledge the financial support from the Polish Ministry of Education and Sciences under Grant 3 T10B 048 30.

References

- [1] Rosenhead L 1931 *Proc. R. Soc. Lond.* **A134** 170
- [2] Clements R R 1976 *AGARD*, Lecture Series no. 86, on *Computational Fluid Dynamics* **5** 1
- [3] Clements R R and Maull D J 1975 *Prog. Aerospace Sci.* **16** 129
- [4] Chorin A J 1973 *J. Fluid Mech.* **57** 785
- [5] Cottet G H and Koumoutsakos P D 2000 *Vortex methods: Theory and Practice*, Cambridge Univ. Press, Cambridge
- [6] Wu J Z, Ma H Y and Zhou M D 2006 *Vorticity and Vortex Dynamics*, Springer
- [7] Greengard L and Rockhlin V 1987 *J. Comp. Phys.* **73** 325
- [8] Kudela H 1995 *Hydrodynamics Phenomena Modelling by Vortex Particles Method*, Wroclaw University of Technology Publishing, Wroclaw (in Polish)
- [9] Christiansen J P 1973 *J. Comp. Phys.* **13** 363
- [10] Cottet G H, Michaux B, Ossia S and VanderLinden G 2002 *J. Comp. Phys.* **175** 702
- [11] Cottet G H and Poncet P 2003 *J. Comp. Phys.* **193** 136
- [12] Mas-Gallic S 1991 *Lectures in Applied Mathematics* **28** 433
- [13] Koumoutsakos P D 1993 *Direct Numerical Simulations of Unsteady Separated Flows Using Vortex Methods*, PhD Thesis, California Institute of Technology, Pasadena, California
- [14] Bradshaw P 1996 *Prog. Aerospace Sci.* **32** 572
- [15] Weinan E and Jian-Guo Liu 1996 *J. Comp. Phys.* **124** 368
- [16] Lightill M J 1963 *Laminar Boundary Layers* (Rosenhead J, Ed.), Oxford University Press, pp. 46–109
- [17] Peyret R and Taylor T D 1983 *Computational Methods for Fluid Flow*, Springer-Verlag, Berlin
- [18] Kudela H and Kozłowski T 2008 *Vortex in Cell Method for Exterior Problems*, Preprint
- [19] Ould-Salhi M L, Cottet G H and El Hamraout M 2000 *J. Sci. Comput.* **22** 1655
- [20] Koumoutsakos P, Leonard A and Pepin F 1994 *J. Comp. Phys.* **113** 52

- [21] Proskurowski W and Widlund O 1976 *Math. Comput.* **30** 433
- [22] Schumann U and Sweet R A 1976 *Lectures Notes in Physics* **59** 397
- [23] White F M 1999 *Fluid Mechanics*, McGraw-Hill
- [24] Ghia U, Ghia K N and Shin C T 1982 *J. Comp. Phys.* **48** 387
- [25] Gresho P M, Chan S T and Lee R L 1984 *Int. J. Numer. Meth. in Fluids* **4** 619
- [26] Kosma Z and Noga B 2006 *Chemical and Process Engng* **27** 761
- [27] Kudela H 1999 *TASK Quart.* **3** 343
- [28] Osswald G A, Ghia K N and Ghia U 1983 *AIAA, 6th CFD Conf.*, Danvers, pp. 686–705
- [29] Armaly B F, Durst F, Pereira J C F and Schonung B 1983 *J. Fluid Mech.* **127** 476
- [30] Orlandi P 1990 *Phys. Fluids A* **2** 1429
- [31] Doligalski T L 1994 *Ann. Rev. Fluid Mech.* **26** 573
- [32] Kudela H and Malecha Z M 2006 *Chemical and Process Engng* **27** 707
- [33] Kudela H and Malecha Z M 2007 *J. Theor. Appl. Mech.* **45** 785
- [34] Smith C R and Walker J D A 1996 *Fluid Vortices* (Green S I, Ed.), Kluwer, Amsterdam, pp. 235–290
- [35] Cottet G H 2000 *Vortex Methods* (T Kamemoto K, Tsutahara M, Eds.), Word Scientific, Singapore, pp. 123–134
- [36] Kudela H and Regucki P 2004 *Computational Science – ICCS 2004, LNCS 3037* (Bubak M, Van Albada G D, Sloot P M A, Dongarra J J, Eds.), Springer-Verlag, Berlin, pp. 356–363
- [37] Ploumhans P, Winckelmans G S, Salmon J K, Leonard A and Warren M S 2002 *J. Comp. Phys.* **178** 427